NeuroImage **11,** 684–696 (2000)
doi:10.1006/nimg.2000.0548, available online at http://www.idealibrary.com on IDEAL®

# Areas 3a, 3b, and 1 of Human Primary Somatosensory Cortex

## 2. Spatial Normalization to Standard Anatomical Space

Stefan Geyer,* Thorsten Schormann,* Hartmut Mohlberg,‡ and Karl Zilles*,†,‡

**Department of Neuroanatomy and †C. and O. Vogt Brain Research Institute, University of Düsseldorf, P.O. Box 10 10 07, 40001 Düsseldorf, Germany; and ‡Institute of Medicine, Research Center Jülich, 52425 Jülich, Germany*

Received September 16, 1999

**Interindividual topographical variability of cytoarchitectonically defined somatosensory areas 3a, 3b, and 1 was analyzed in the standard anatomical format of a computerized brain atlas. T1-weighted magnetic resonance images were obtained from 10 postmortem brains. The brains were serially sectioned at 20 μm, sections were stained for cell bodies, and areas 3a, 3b, and 1 were defined with an observer-independent cytoarchitectonic technique. After correction of the sections for deformations due to histological processing, the 3-D reconstructed histological volumes of the individual brains and the volume representations of the cytoarchitectonic areas were adapted to the reference brain of a computerized atlas. Corresponding areas were superimposed in the 3-D space of the reference brain. These population maps describe, for each voxel, how many brains have a representation of one particular cytoarchitectonic area. Each area's extent is very variable across different brains, but representations of areas 3a, 3b, and 1 in ≥50% of the brains were found in the fundus of the central sulcus, its caudal bank, and on the crown of the postcentral gyrus, respectively. Volumes of interest (VOIs) were defined for each area in which ≥50% of the brains have a representation of that area. Despite close spatial relationship of areas 3a, 3b, and 1 in the postcentral gyrus, the three VOIs overlap by <1% of their volumes. Functional imaging data can now be brought into the same standard anatomical format, and changes in regional cerebral blood flow can be calculated in VOIs of areas 3a, 3b, and 1, which are derived from genuine cytoarchitectonic data.** © 2000 Academic Press

## INTRODUCTION

In a previous article (Geyer *et al.*, 1999), the cytoarchitectonic borders of areas 3a, 3b, and 1 of the human primary somatosensory cortex were identified with a new observer-independent and statistically testable procedure (Schleicher *et al.*, 1999) in 10 postmortem brains. Significant changes in cytoarchitecture were detected at corresponding positions across a series of nearby sections in each brain. These borders matched visible changes in cytoarchitecture in cell-stained sections. Area 3a lies in the fundus of the central sulcus, and area 3b in the rostral bank of the postcentral gyrus (or posterior bank of the central sulcus). Area 1 occupies the crown of the postcentral gyrus and reaches down into the postcentral sulcus.

Plenty of evidence in nonhuman primates shows that cytoarchitectonic areas are also functional entities (see, e.g., Matelli *et al.*, 1991; Luppino *et al.*, 1991). *Macrostructural landmarks* yield clues as to the *approximate location* of a cortical area, i.e., fundus of the central sulcus, area 3a; rostral bank of the postcentral gyrus (or posterior bank of the central sulcus), area 3b; and crown of the gyrus, area 1. *Borders* of cortical areas, however, can only be detected by *microstructural analysis.* There are no dimples, notches, or grooves that mark these borders reliably across a series of individual brains. Thus, areal borders and the extent of most cortical areas cannot be identified in high-resolution magnetic resonance images. This leaves a substantial degree of uncertainty when, based only on macroanatomical landmarks of the postcentral gyrus, investigators attempt to assign activation foci in positron emission tomography (PET) or functional magnetic resonance imaging (fMRI) scans to cytoarchitectonic areas.

For a solution of this problem, the atlas of Talairach and Tournoux (1988) is only of limited value. The authors used Brodmann's (1909) nomenclature of cortical areas, but the atlas is based on one brain only, which "was not subjected to histologic studies and the transfer of the cartography of Brodmann usually pictured in two-dimensional projections sometimes possesses uncertainties" (Talairach and Tournoux, 1988, p. 10). The authors seem to have transferred each area from Brodmann's schematic drawing to a corresponding position on the cortex of the Talairach brain. This allows only an approximate description of each area's location, since interareal borders were not defined. Further-



1053-8119/00 $35.00

**TABLE 1**

Histological Processing and Cytoarchitectonic Analysis, 3-D Reconstruction of the Histological Volume, and Spatial Normalization

Ten postmortem human brains, fixed in formalin or Bodian's fixative for several months (cf. Fig. 1A)
↓
T1 weighted MR scan (1.5 T Siemens scanner; 3-D FLASH sequence) (→ MR volume)
↓
Dehydrating in graded alcohols and embedding in paraffin
↓
Serial whole brain sections (20 μm thick; coronal plane) (cf. Fig. 1B)

| Histological sections | Images of paraffin blockface |
|---|---|
| ↓ | & |
| Mounting on coated slides | Digitized histological sections |
| ↓ | & |
| Cell stain with modified silver method | MR volume of the same brain |
| ↓ | ↓ |
| Cytoarchitectonic analysis | |
| ↓ | |
| Delineation of cortical areas (cf. Fig. 1B) | |
| Transfer (cf. Fig. 1D) | 3-D reconstruction of the histological volume (cf. Fig. 1C) |

Spatial normalization of the 3-D reconstructed histological volume and areas to the reference brain of the computerized atlas (cf. Figs. 2B–D)
↓
Superimposition of normalized histological volumes (cf. Figs. 3A–B) and areas in 3-D space
↓
Population map for each cortical area (cf. Figs. 4B–D)

**TABLE 2**

Brains Used for Spatial Normalization of Areas 3a, 3b, and 1

| Brain | Sex | Age (years) | Cause of death | Post mortem delay (hours) | Fixative |
|---|---|---|---|---|---|
| 207/84 | Male | 75 | Toxic glomerulo-nephritis | 24 | Formalin |
| 544/91 | Female | 79 | Carcinoma of the bladder | 24 | Bodian |
| 281/93 | Male | 68 | Vascular disease | 16 | Formalin |
| 189/92 | Male | 55 | Carcinoma of the rectum | 24 | Formalin |
| 68/95 | Female | 79 | Cardiorespiratory insufficiency | 16 | Bodian |
| 2/95 | Female | 85 | Mesenteric artery infarction | 14 | Bodian |
| 56/94 | Female | 72 | Renal failure | 12 | Formalin |
| 2431 | Male | 39 | Drowning | 10 | Formalin |
| 146/86 | Male | 37 | Right heart failure | 24 | Formalin |
| 16/96 | Male | 54 | Myocardial infarct | 8 | Formalin |

more, Brodmann's map shows each area on the free cortical surface only. Approximately 60% of the cortex, however, is buried in the depths of the sulci (Zilles *et al.*, 1988). In addition, analysis of only one brain does not address the problem of interindividual variability of cortical areas. Thus, the validity of the "Brodmann areas" as delineated in the Talairach atlas must be seriously questioned.

These problems can be solved by using a MRI-based brain atlas (Roland and Zilles, 1994, 1996a) which maintains the original 3-D format of the data and displays genuine microstructural and functional data that were spatially normalized to its reference brain. This reference brain is a common spatial reference system to assess the degree of interindividual microstructural variability (Geyer *et al.*, 1996; Roland *et al.*, 1997; Roland and Zilles, 1998; Amunts *et al.*, 1999a, 1999b) and to correlate microstructural with functional imaging data (Geyer *et al.*, 1996; Roland and Zilles, 1998; Naito *et al.*, 1999).

In the previous paper (Geyer *et al.*, 1999), somatosensory areas 3a, 3b, and 1 were cytoarchitectonically delineated in 10 postmortem brains. In this study, these areas are spatially normalized to the reference brain of the computerized Human Brain Atlas (Roland and Zilles, 1994, 1996a), with an approach based on a new extended principal axes theory and a fast automated multiresolution full-multigrid movement model (Schormann and Zilles, 1997, 1998). Corresponding areas from different brains are superimposed in 3-D space to show the degree of interindividual topographical variability. This is the prerequisite for *probabilistic microstructural–functional correlation* with, e.g., PET data (Geyer *et al.*, 1996; Roland and Zilles, 1998; Naito *et al.*, 1999).

## MATERIALS AND METHODS

The flowchart in Table 1 gives an overview of the procedure: (i) histological processing and cytoarchitec-

**FIG. 1.** (A) Postmortem brain 207/84 after fixation for 5 months in formalin. (B) Coronal section 3061 through A (cf. dashed line in A; thick arrow indicates direction of sectioning). Cytoarchitectonic areas 3a, 3b, and 1 are marked, as defined by observer-independent delineation of cytoarchitectonic borders. (C) 3-D reconstructed histological volume of brain 207/84. (D) Coronal section through C (cf. dashed line in C), which corresponds to histological section 3061 shown in B. Areas 3a, 3b, and 1 were labeled according to each area's extent in the histological section (cf. B). Frontal is to the left and occipital to the right in A and C. L, left hemisphere; R, right hemisphere; cs, central sulcus.

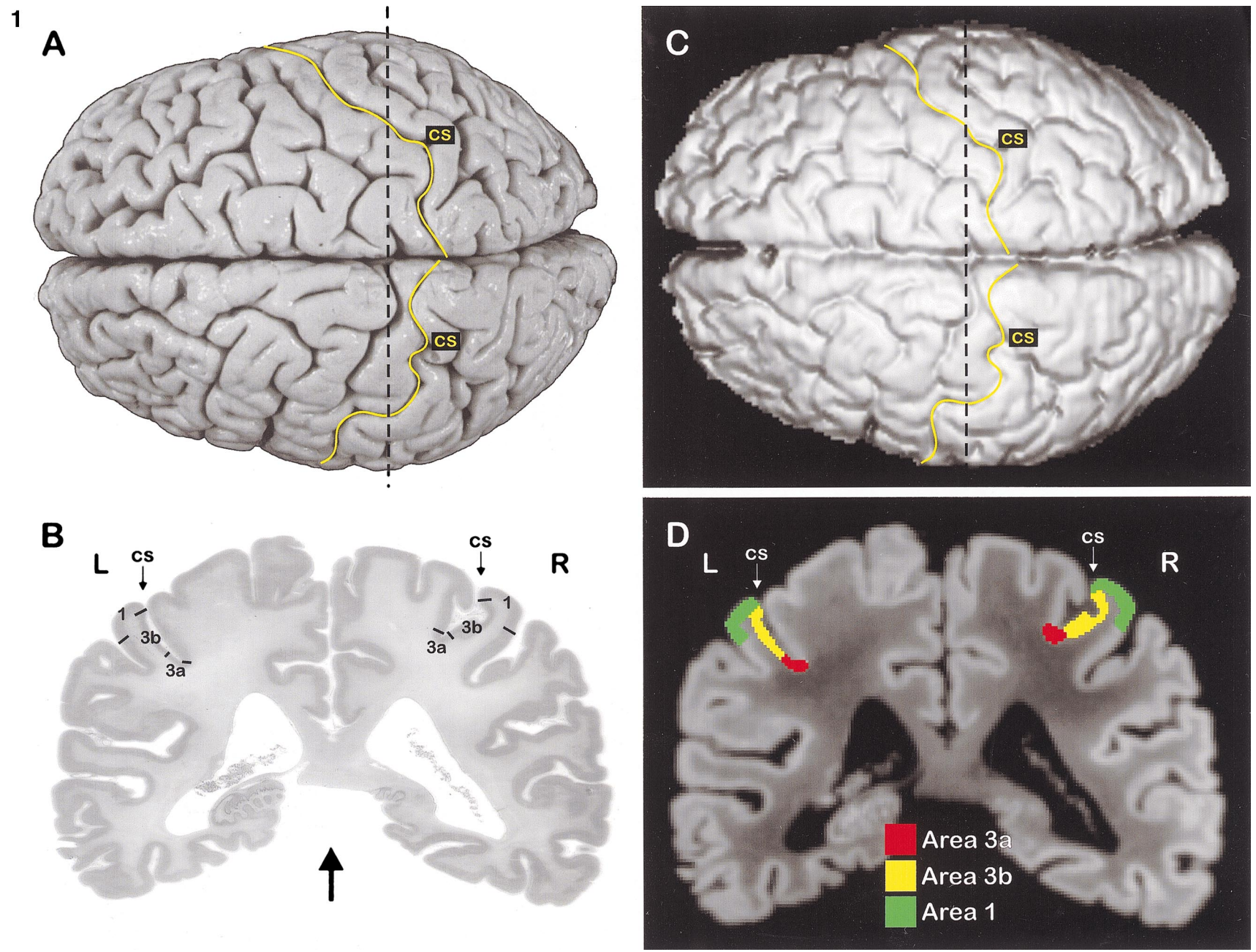
1
A
CS
CS
B
L
CS
1
3b
3a
CS
R
1
3b
3a
C
CS
CS
D
L
CS
CS
R
Area 3a
Area 3b
Area 1

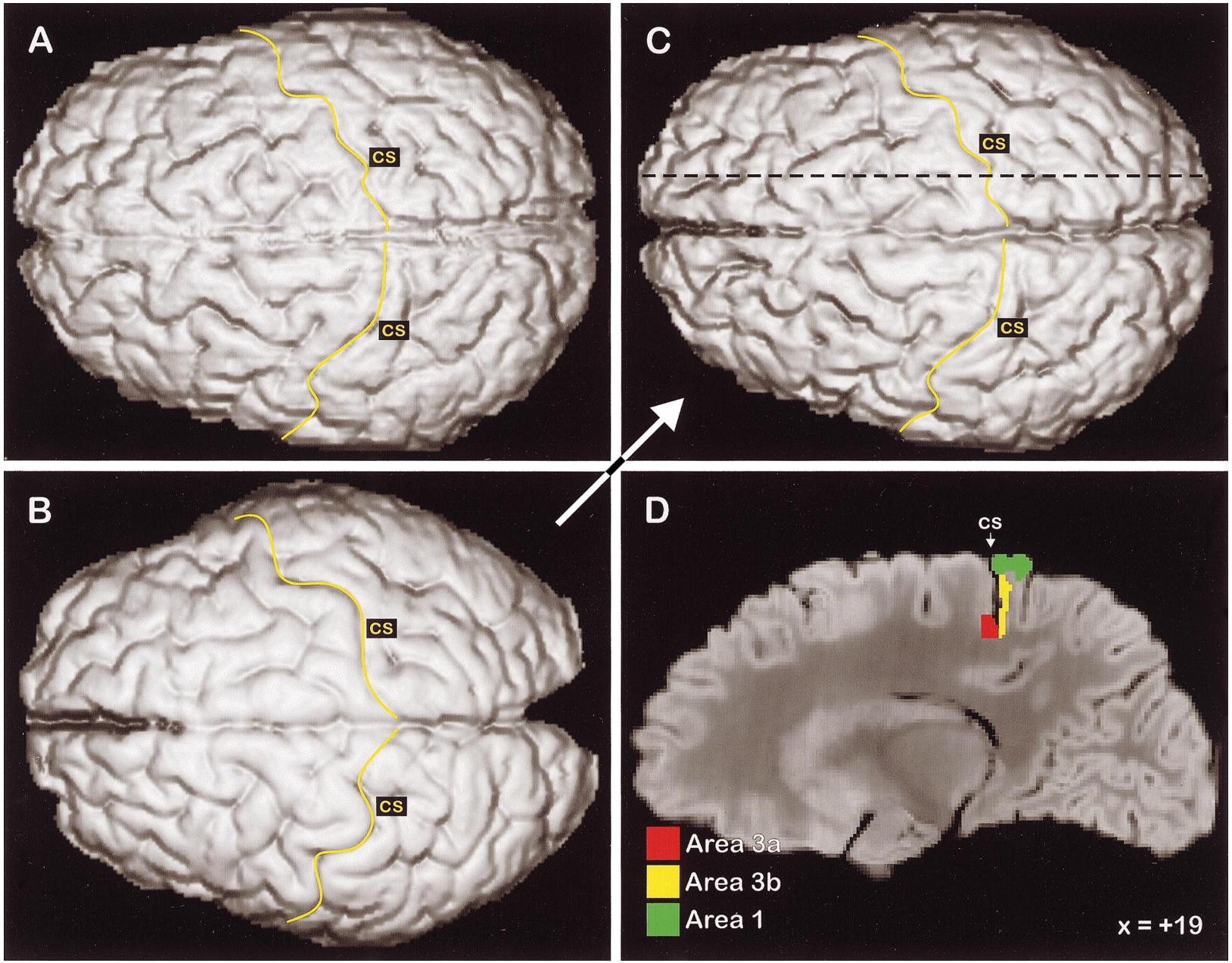


**FIG. 2.** (A) Reference brain of the computerized atlas. (B, C) 3-D reconstructed histological volume of brain 68/95 prior to (B) and after (C) spatial normalization to the reference brain (cf. gyral and sulcal patterns in A and C). (D) Sagittal section through C at x = +19 (cf. dashed line in C) with areas 3a, 3b, and 1. For other conventions and abbreviations see Fig. 1.

tonic analysis (top and left), (ii) 3-D reconstruction of the histological volume (right), and (iii) spatial normalization (bottom).

### *Histological Processing and Cytoarchitectonic Analysis*

The histological processing and cytoarchitectonic analysis have been described in detail in the previous article (Geyer *et al.*, 1999). Only major points will be summarized here. The cytoarchitectonic analysis was done in 10 postmortem brains obtained at autopsy from subjects with no known history of neurological or psychiatric diseases (6 males and 4 females, mean age 64.3 years, range 37–85 years; cf. Table 2). All subjects were included in the body donor program of the Anatomical Institute (University of Düsseldorf, Germany). The brains were fixed in 4% formaldehyde or in Bodian's fixative (90 ml of 80% ethanol, 5 ml of 37% formaldehyde, and 5 ml of glacial acetic acid) for 5 months. They were suspended at the basilar artery to avoid compression during fixation. T1-weighted MRI scans (1.5 T Siemens Magnetron SP scanner; 3-D fast, low angle shot (3-D FLASH) pulse sequence; flip angle = 40°; TR = 40 ms; TE = 5 ms; voxel size = 1.17 mm (mediolateral) × 1 mm (rostrocaudal) × 1 mm (dorsoventral)) were acquired for documentation of brain size and shape before subsequent histological processing, which induces shrinkage and distortions. The brains were dehydrated in graded alcohols, embedded in paraffin, and sectioned coronally (20-μm whole brain sections) with a microtome for large sections. Images of the paraffin blockface were obtained after each 60th section with a CCD camera (image matrix: 256 × 256 pixels; 8 bit grey value resolution). Each 60th section was mounted on a gelatin-coated slide and was stained for cell bodies with a modified silver method (Merker, 1983), which yields high-contrast staining of cell bodies for cytoarchitectonic analysis and delineation of areas 3a, 3b, and 1 in both hemispheres (see Geyer *et al.*, 1999).

### *3-D Reconstruction of the Histological Volume*

Each mounted and cell-stained histological section was digitized with a CCD camera (image matrix: 256 × 256 pixels; 8 bit grey value resolution). The histological volume of the brain was then reconstructed in 3-D from (i) the images of the paraffin blockface (for proper alignment of the sections), (ii) the digitized histological sections (for demonstration of the microstructure), and (iii) the MR volume of the same brain (for correction of distortions) with linear and nonlinear transformations (Schormann *et al.*, 1993, 1995, 1996, 1997; Schormann and Zilles, 1997, 1999). Since the MR volume was obtained prior to histological processing, any artifacts (e.g., shrinkage of the brain due to dehydration in graded alcohols or compression of the sections due to cutting) could be eliminated in the 3-D reconstructed histological volume by matching with the MR volume of the same brain. An image analysis software package with an interactive voxel-painting program (KS 400, Version 3.0; Zeiss, Germany) was used to label the extent of areas 3a, 3b, and 1 in the images of corresponding sections of the reconstructed volume according to each area's borders, which had been detected in each histological section by observer-independent delineation of cytoarchitectonic borders. With this approach, a microstructurally defined representation of cytoarchitectonic areas 3a, 3b, and 1 was obtained in the 3-D reconstructed histological volume of each brain.

### *Spatial Normalization*

Each 3-D reconstructed histological volume (with areas 3a, 3b, and 1) was spatially normalized to the reference brain (which is oriented in the Talairach coordinate system, viz Roland *et al.*, 1994) of the computerized Human Brain Atlas with an approach based on a new extended principal axes theory (PAT; Schormann *et al.*, 1997) and a fast automated multiresolution full-multigrid movement model (Schormann and Zilles, 1997, 1998).

The system of transformations is applied in a hierarchical manner from coarse to fine thereby combining low and high dimensional transformations. In a first step, the individual histological volumes are transformed to the reference brain with an extended PAT generalized to affine transformation parameters. This theory extends the classical PAT to non-rigid linear transformations which are at least one order of magnitude more accurate than the results of the classical PAT (Schormann and Zilles, 1997). This technique is insensitive to noise or to symmetries of objects and does not require any interactive support for correlating corresponding landmarks (e.g., points, lines, or surfaces) in both volumes. Such a global or coarse registration accounts for differences in scaling (size), rotation (orientation), translation (position), and shearing which result from different eigensystems of both volumes (Schormann *et al.*, 1993). The extended PAT precisely aligns objects on the basis of linear parameters which is an important prerequisite for the nonlinear refinement by a fast automated full-multigrid movement technique (Schormann and Zilles, 1997, 1998). The histological volumes are modeled as elastic material whereby the transformation to the reference brain is smooth so that connected regions remain connected and global relationships between structures are maintained. In order to account for large deformations, it is necessary to extend the elastic model to a movement model whereby the histological volume is deformed iteratively by using the result of the previous iteration for the next step until a satisfactory match is achieved.

High dimensional transformations with up to 24 million degrees of freedom were used for the histological volumes in order to account for the different morphology between individual and reference brain whereby the transformations of the coarse and fine stage were determined without any interactive support. High dimensional and linear transformations were combined and applied to each 3-D reconstructed histological volume with areas 3a, 3b, and 1.

The 10 normalized histological volumes were superimposed in the 3-D space of the reference brain. Population maps were generated for corresponding areas from different brains, which show the degree of interindividual microstructural variability by exemplifying, for each voxel, how many brains have a representation of one particular cytoarchitectonic area. For quantitative analysis, the data from the left and right hemispheres were pooled.

## RESULTS

Figure 1A shows a dorsal view of postmortem brain 207/84 after fixation for 5 months in formalin. The brain was then scanned with a 3-D FLASH pulse sequence, subsequently embedded in paraffin, and sectioned coronally (20-μm whole brain sections) with a microtome for large sections. Then 7561 sections were obtained from this brain. Each 60th section was mounted and stained for cell bodies with a modified silver method. Section 3061 is shown in Fig. 1B (cf. dashed line in Fig. 1A). Areas 3a, 3b, and 1 are marked, as defined by observer-independent identification of cytoarchitectonic borders (see Geyer *et al.*, 1999). The 3-D reconstructed histological volume of brain 207/84 is shown in Fig. 1C, and a coronal section through this volume that corresponds to section 3061 is shown in Fig. 1D (cf. dashed line in Fig. 1C). Areas 3a, 3b, and 1 were labeled interactively in images of coronal sections of the reconstructed histological volume according to each area's extent in the corresponding cell-stained sections (cf. Figs. 1B and 1D).

Each 3-D reconstructed histological volume was then spatially normalized to the reference brain (volume rendering shown in Fig. 2A) of the computerized atlas. The histological volume of brain 68/95 is depicted prior to normalization in Fig. 2B and after normalization in Fig. 2C. After spatial normalization the gyral and sulcal pattern of brain 68/95 (Fig. 2C) matches the pattern of the reference brain (Fig. 2A). A sagittal section through the normalized histological volume of brain 68/95 with areas 3a, 3b, and 1 is shown in Fig. 2D ($x = +19$; cf. dashed line in Fig. 2C).

The normalized histological volumes of all 10 brains were then aligned in 3-D space and superimposed. A mean brain was generated in which each voxel represents the arithmetic mean of the grey values of the superimposed histological volumes (volume rendering of the mean brain shown in Fig. 3A and sagittal section at $x = +16$ (cf. dashed line in Fig. 3A) in Fig. 3B). Corresponding views of the reference brain are depicted in Figs. 3C (volume rendering) and 3D (sagittal section at $x = +16$ (cf. dashed line in Fig. 3C)). There is a good match between the gyral and sulcal patterns of the mean brain and the reference brain.

Population maps were generated for corresponding areas from the 10 normalized histological volumes. Figures 4B–4D depict the population maps of areas 3a, 3b, and 1, respectively (right hemisphere; $x = +49$; reference brain (cf. Fig. 4A) is shown in the background). These population maps describe, for each voxel, how many brains have a representation of one particular cytoarchitectonic area. This representation is color coded in a spectral sequence from dark blue (area is present in only 1 of 10 brains in this voxel) to dark red (in all 10 brains). Despite considerable interindividual variability, a clear focus is obvious for each area. The focus of area 3a lies in the depth of the central sulcus toward its fundus (Fig. 4B), the focus of area 3b in the rostral bank of the postcentral gyrus (or posterior bank of the central sulcus; Fig. 4C), and the focus of area 1 on the crown of the postcentral gyrus (Fig. 4D).

The volume of each area's representation (in both hemispheres) in 1 of 10 brains is 13.64 $cm^3$ for area 3a, 23.09 $cm^3$ for area 3b, and 18.16 $cm^3$ for area 1 (Fig. 5A). Conversely, the volume of each area's representation (both hemispheres) in ≥5 of 10 brains is 1.68 $cm^3$ for area 3a, 4.02 $cm^3$ for area 3b, and 7.34 $cm^3$ for area 1. If each area's entire representation (in ≥1 of 10 brains) in both hemispheres is defined as 100% (Fig. 5B), the representation in 1 of 10 brains is 53.77% for area 3a, 44.45% for area 3b, and 42.41% for area 1, whereas the representation in ≥5 of 10 brains is 6.61% for area 3a, 7.72% for area 3b, and 17.18% for area 1 (exploded pie slices in Fig. 5B).

The volume of each area's representation in a small number of brains (1 of 10, 2 of 10, etc.) is large. Conversely, each area's representation in a large number of brains is relatively small. When superimposing the population maps of *all three areas* in 3-D space, it is impossible to *unequivocally* assign many voxels in standard anatomical space to area 3a or area 3b or area 1 due to considerable interindividual variability on the one hand and the close spatial relationship of the three areas in the postcentral gyrus on the other hand. This problem arises, however, when *nonoverlapping* volumes of interest (VOIs) are to be defined for each area (e.g., for measurements of changes in regional cerebral blood flow in these microstructural VOIs in PET or fMRI data which have been brought into the same spatial format). A representation of each area in ≥50% of the brains is an adequate compromise between a sufficiently large VOI of each area and a minimal number of overlapping voxels between adjacent VOIs (area

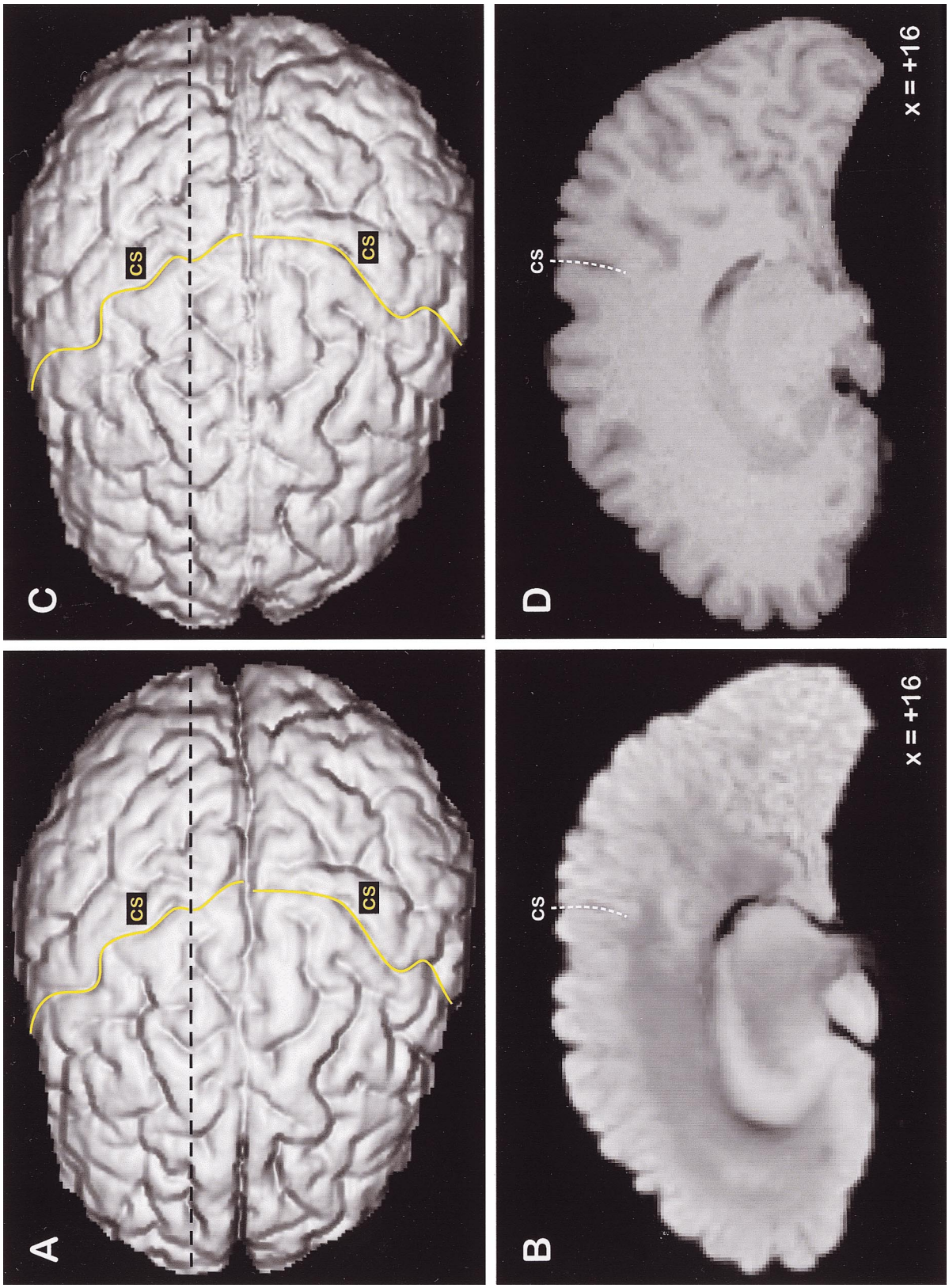


**FIG. 3.** (A) Mean brain calculated from the spatially normalized and superimposed histological volumes of all 10 brains. (B) Sagittal section through A at x = +16 (cf. dashed line in A). (C) Reference brain of the computerized atlas. (D) Sagittal section through C at x = +16 (cf. dashed line in C). For other conventions and abbreviations see Fig. 1.

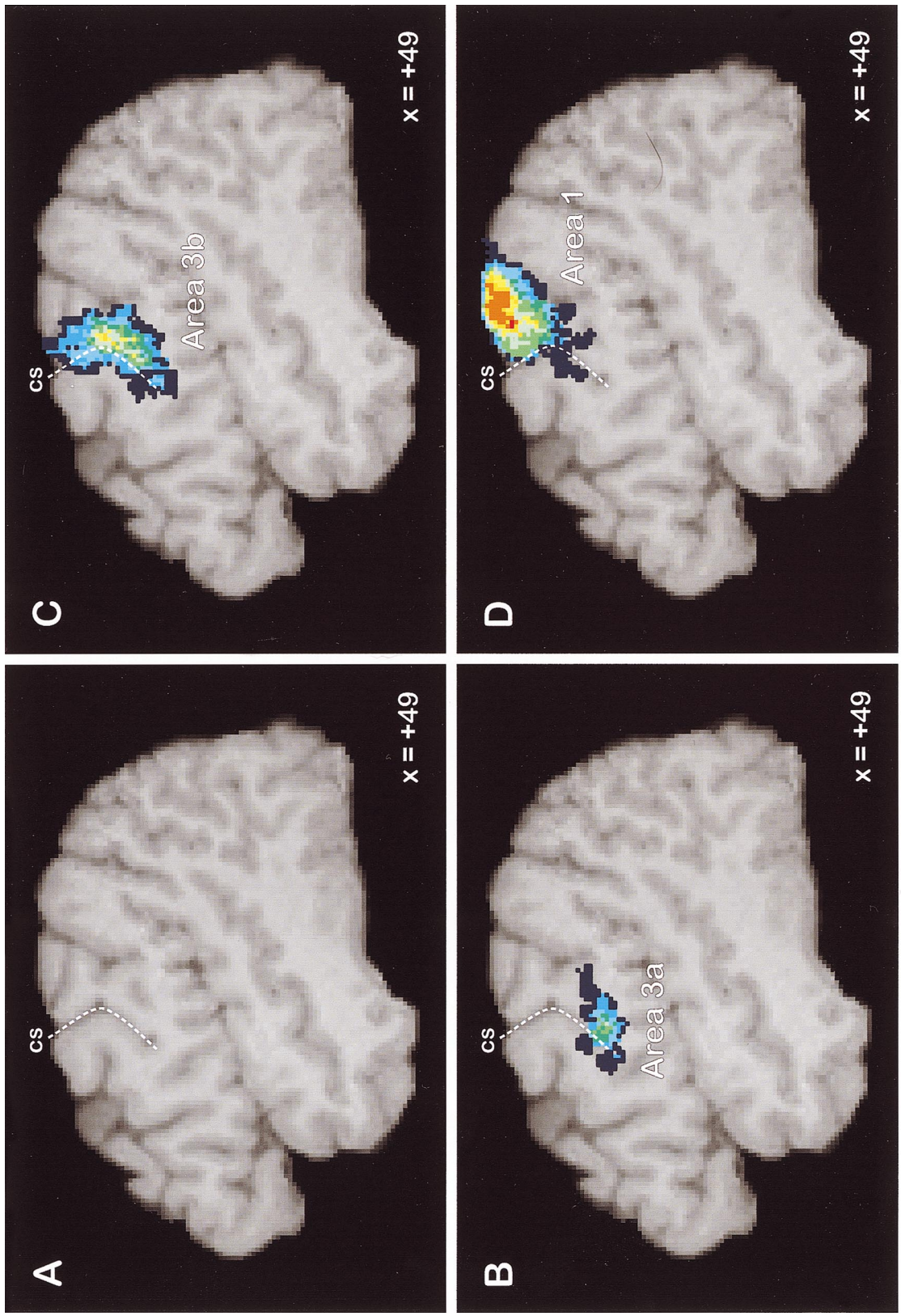


**FIG. 4.** (A) Sagittal section through reference brain at x = +49. (B–D) Population maps of areas 3a (B), 3b (C), and 1 (D) at x = +49 (right hemisphere). For other conventions and abbreviations see Fig. 1.

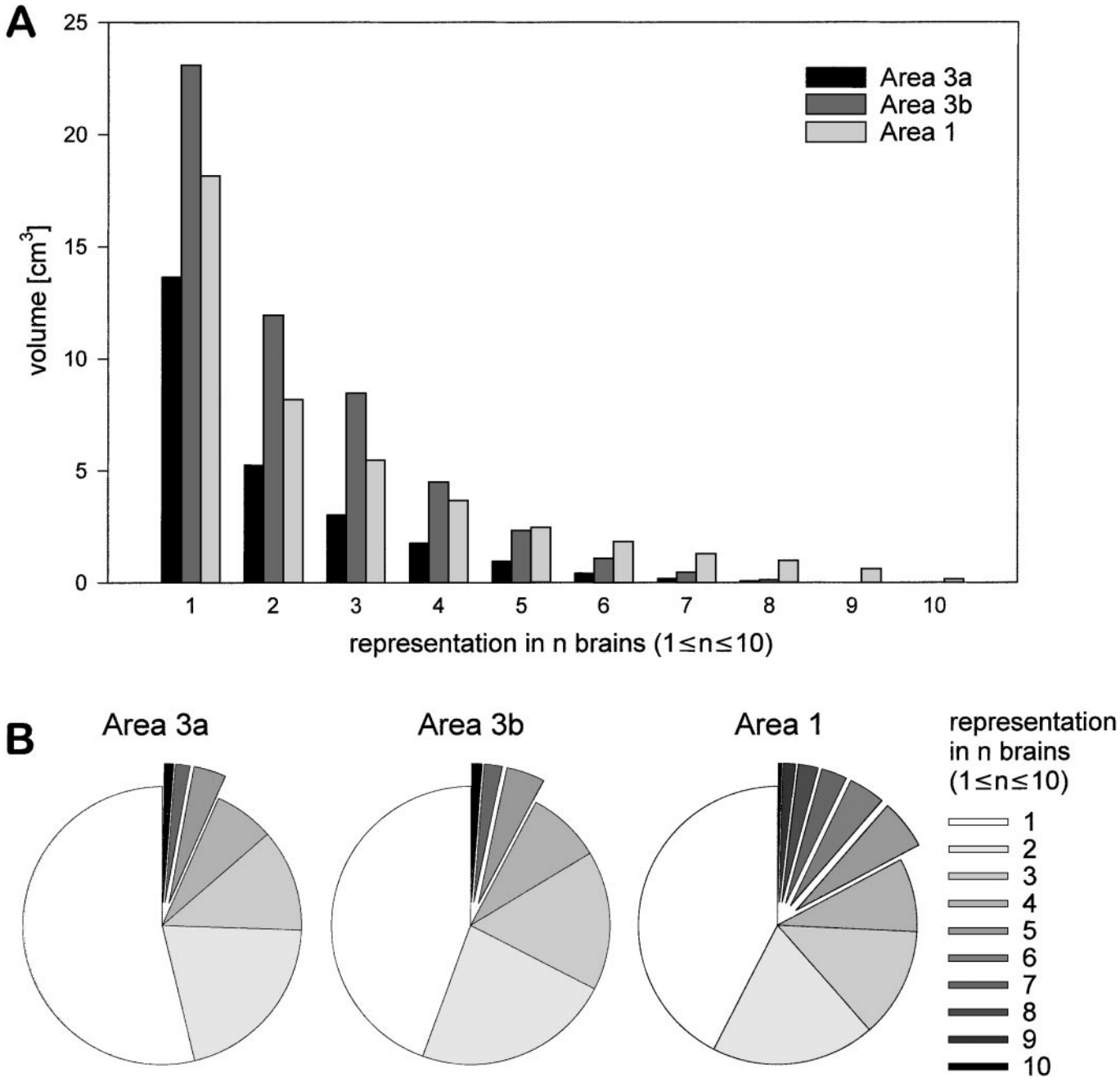


**FIG. 5.** (A, B) Volumes of each area's representations in n brains ($1 \leq n \leq 10$; both hemispheres) in $cm^3$ (A) and relative to each area's entire representation (in ≥1 of 10 brains; both hemispheres; B). Each area's representations in ≥5 of 10 brains are shown as exploded slices in B.

3a ∩ area 3b, area 3b ∩ area 1). Figure 6A shows each area's VOI for ≥5 of 10 brains at $x = +49$ (right hemisphere). Overlapping voxels between the VOIs of areas 3a and 3b are color coded in pink, between the VOIs of areas 3b and 1 in orange. Each VOI's volume (in $cm^3$) in both hemispheres is depicted in Fig. 6B. Volumes of overlap between adjacent VOIs are minimal (area 3a ∩ area 3b, 0.059 $cm^3$ or 0.46% of the total volume of all three VOIs in both hemispheres (cf. Fig. 6C); area 3b ∩ area 1, 0.083 $cm^3$ or 0.64% of the total volume of all three VOIs in both hemispheres (cf. Fig. 6C)).

## DISCUSSION

In this study somatosensory areas 3a, 3b, and 1, which had been cytoarchitectonically delineated in 10 postmortem brains (Geyer *et al.*, 1999), were spatially

normalized to the reference brain of the computerized Human Brain Atlas (Roland and Zilles, 1994, 1996a). Corresponding areas from different brains were superimposed in 3-D space, and population (or probability) maps were generated for each area which show the degree of microstructural interindividual variability. On this basis, microstructural and functional imaging data can be correlated in a probabilistic way.

Microstructural–functional correlation is validated by many findings in nonhuman primates, which show that cortical areas as functional entities can be defined *only* on a microstructural basis, e.g., by cytoarchitecture. In humans, however, the situation is more complex, since interareal borders do not match macrostructural landmarks of the cortex, and they vary considerably in their positions relative to these landmarks across different brains (Rademacher *et al.*, 1993; Roland and Zilles, 1994; Rajkowska and Goldman-Rakic, 1995; Geyer *et al.*, 1996, 1999; Roland and Zilles, 1996b; White *et al.*, 1997; Roland *et al.*, 1997; Amunts *et al.*, 1999a). In addition, in humans, unlike in monkeys, functional and postmortem microstructural studies cannot be performed in the same brain. Published atlases, e.g., the atlas of Talairach and Tournoux (1988), are of limited value in this respect, as their cortical maps are not based on genuine microstructural data, they give only the approximate position of an area, and they do not address the problem of interindividual variability.

The procedure outlined in this article is an approach to overcome these problems. Genuine microstructural data (e.g., cytoarchitectonic analysis of cell-stained sections obtained from postmortem brains) are brought into the standard anatomical format of the atlas. The degree of interindividual variability can be assessed by importing microstructural data from several brains (approximately 10 in order to keep the time-consuming and cumbersome procedure of microstructural parcellation within reasonable limits). Functional imaging data can then be brought into the identical standard anatomical format, superimposed with the microstructural data, and correlated with them on a probabilistic basis.

Macrostructural variability between brains is well known and has been extensively documented in the recent literature (Ono *et al.*, 1990; Loftus *et al.*, 1995; Thompson *et al.*, 1996; Penhune *et al.*, 1996; Paus *et al.*, 1996a, 1996bs; White *et al.*, 1997; Bartley *et al.*, 1997; Zilles *et al.*, 1997; Kennedy *et al.*, 1998; Leonard *et al.*, 1998; Varnavas and Grand, 1999; Westbury *et al.*, 1999; Tomaiuolo *et al.*, 1999). Unfortunately, the biological rules of genetics and development are complex and the differential contributions of genetic and environmental factors (Bartley *et al.*, 1997), which lead to this diversity are largely unknown. Hence, no *a priori* mathematical model of choice that adequately describes these underlying factors is currently available.

All relatively simple models with finite numbers of parameters are only an approximation of this complexity. When different brains are normalized with the proportional grid system of Talairach and Tournoux (1988), considerable residual macroanatomical variability remains, e.g., in the rostrocaudal position of the central sulcus (see Fig. 7 of Talairach and Tournoux, 1988).

Therefore, in this study a new and mathematically more powerful warping technique was used which does not require any user interaction (since interactive approaches to normalize brains cannot be reproduced across different investigators and the quality of fit depends on each investigator's experience). The approach is based on a new extended principal axes theory and a fast automated multiresolution full-multigrid movement model (Schormann and Zilles, 1997, 1998). The power and accuracy of this new technique in comparison with other warping approaches was recently tested (Crivello *et al.*, 1999) with 20 MRI volumes (1.5 T GE Horizon LX scanner; T1 weighted spoiled gradient sequence), which were spatially normalized to the reference brain with four different warping techniques: (i) a simple nine parameter model, (ii) the nonlinear procedure implemented in the statistical parametric mapping (SPM) package (Ashburner and Friston, 1997), (iii) the 5th order (168 parameters) nonlinear warping algorithm included in the automated image registration (AIR) tool (Woods *et al.*, 1998), and (iv) the multiresolution full-multigrid movement model (FMG; which was used in this study). The adjusted mean MRI volume across the 20 subjects was computed for each procedure, and difference volumes (mean $\text{volume}_{\text{SPM}}$ − mean $\text{volume}_{\text{FMG}}$ and mean $\text{volume}_{\text{SPM}}$ − mean $\text{volume}_{\text{AIR}}$) were generated. The difference volumes revealed that the SPM and AIR algorithms performed similarly whereas the FMG approach dramatically improved the spatial accuracy with which each individual brain was adapted to the reference brain (Crivello *et al.*, 1999). Hence, the residual macroanatomical variability is dramatically reduced (although not eliminated altogether) with this new FMG approach. Figure 3B shows a sagittal section through the mean brain generated from the 10 normalized histological volumes. The outer contour and the ventricular surface are sharp but sulci and subcortical nuclei are slightly blurred. It can therefore be assumed that each area's "interindividual variability" as shown in the population maps is due to minimal residual macroanatomical variability but the rest is indeed microstructural in nature.

Considerable interindividual microstructural variability leads to overlapping regions when population maps of areas with close spatial relationship in the cortex are superimposed in standard anatomical space. It is impossible to unequivocally assign many voxels to a given area. Despite considerable variability, how-

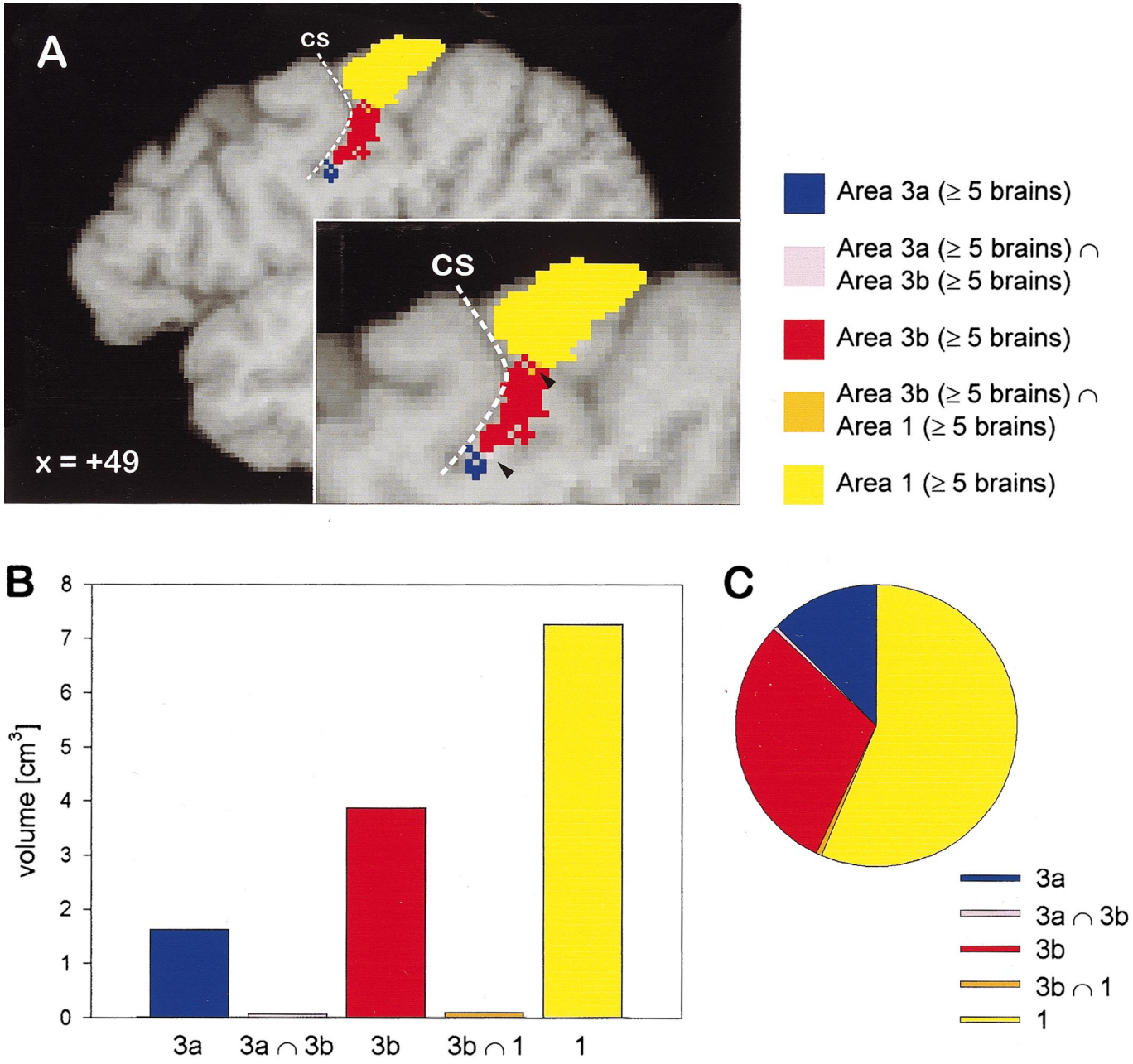


**FIG. 6.** (A) Each area's VOI (representation in ≥5 of 10 brains) at x = +49 (right hemisphere). Overlapping voxels between VOIs of anatomically adjacent areas (arrowheads) are color coded in pink (area 3a ∩ area 3b) and orange (area 3b ∩ area 1). For other conventions and abbreviations see Fig. 1. (B, C) Volumes of each area's VOI (representation in ≥5 of 10 brains; both hemispheres) and volumes of overlap between VOIs of adjacent areas in $cm^3$ (B) and relative to the entire volume of all three VOIs (C).

ever, clear foci are obvious for each area in cortical regions which are in accordance with the published literature (area 3a in the ascending part of the postcentral gyrus close to the fundus of the central sulcus, area 3b in the rostral bank, and area 1 on the crown of the postcentral gyrus). Considering each area's representation in an increasing number of brains (≥2 of 10, ≥3 of 10, etc.) considerably reduces the spatial extent of each area's VOI and the number of overlapping voxels between the VOIs of adjacent areas. With a very high number of brains (≥6 of 10, ≥7 of 10, etc.), however, the VOIs of small cortical areas (e.g., area 3a) become exceedingly small (cf. Fig. 5A). In addition, there are increasingly wide gaps (i.e., a microstructural "no man's land") between anatomically adjacent areas. This situation never occurs in an individual brain, as two adjacent areas always have a common border. A representation in ≥5 of 10 brains is an ade-

quate compromise between a sufficiently large VOI of each area and a minimal degree of overlap between adjacent VOIs.

This opens up the exciting possibility of defining VOIs of somatosensory areas 3a, 3b, and 1, which are not based on macroanatomical landmarks but instead on cytoarchitectonic mapping of postmortem brains. Probabilistic microstructural data can now be correlated with probabilistic functional data, i.e., PET or fMRI data can be brought into the same anatomical format of the computerized atlas, and changes in regional cerebral blood flow can be calculated in VOIs that are derived from genuine microstructural analysis. Only from this probabilistic microstructural—functional correlation can we infer whether a PET or fMRI activation engages only one or several adjacent cytoarchitectonic areas of the human cerebral cortex.

### *Technical Note*

The population maps of the microstructure of areas 3a, 3b, and 1 are part of the European Computerized Human Brain Database (ECHBD; Roland *et al.*, 1999). The ECHBD is a 3-D database for relating function to the microstructure of the human cerebral cortex. 3-D images of postmortem brains in which cortical areas have been mapped with quantitative microstructural techniques are available in standard anatomical format, as are 3-D images of statistical maps of PET and fMRI experiments, and equivalent current dipoles from magnetoencephalography (MEG) and electroencephalography (EEG) experiments. The ECHBD is open for use and submission. Researchers can directly compare the localization and extent of their functional activations with the population maps of cytoarchitectural areas and the results from other PET, fMRI, MEG, and EEG experiments. Further details can be found at the ECHBD website: www.dhbr.neuro.ki.se.

## ACKNOWLEDGMENTS

The authors thank U. Blohm and B. Machus for excellent technical assistance. Parts of this work were supported by grants from the Deutsche Forschungsgemeinschaft (SFB 194/A6), the EU BioMed 2 and BioTech programs, and the Human Brain Project.

## REFERENCES

Amunts, K., Malikovic, A., Mohlberg, H., Schormann, T., and Zilles, K. 1999b. Brodmann's areas 17 and 18 brought into stereotaxic space—Where and how variable? In press.

Amunts, K., Schleicher, A., Bürgel, U., Mohlberg, H., Uylings, H. B. M., and Zilles, K. 1999a. Broca's region revisited: Cytoarchitecture and intersubject variability. *J. Comp. Neurol.* **412:**319–341.

Ashburner, J., and Friston, K. 1997. Multimodal image coregistration and partitioning—A unified framework. *Neuroimage* **6:**209–217.

Bartley, A. J., Jones, D. W., and Weinberger, D. R. 1997. Genetic variability of human brain size and cortical gyral patterns. *Brain* **120:**257–269.

Brodmann, K. 1909. *Vergleichende Lokalisationslehre der Großhirnrinde.* Barth, Leipzig.

Crivello, F., Lemazurier, N., Mazoyer, N., and Mazoyer, B. 1999. Comparing spatial normalization procedures. *Neuroimage* **9:**S31.

Geyer, S., Ledberg, A., Schleicher, A., Kinomura, S., Schormann, T., Bürgel, U., Klingberg, T., Larsson, J., Zilles, K., and Roland, P. E. 1996. Two different areas within the primary motor cortex of man. *Nature* **382:**805–807.

Geyer, S., Schleicher, A., and Zilles, K. 1999. Areas 3a, 3b, and 1 of human primary somatosensory cortex: 1. Microstructural organization and interindividual variability. *Neuroimage* **10:**63–83.

Kennedy, D. N., Lange, N., Makris, N., Bates, J., Meyer, J., and Caviness, V. S. 1998. Gyri of the human neocortex: An MRI-based analysis of volume and variance. *Cereb. Cortex* **8:**372–384.

Leonard, C. M., Puranik, C., Kuldau, J. M., and Lombardino, L. J. 1998. Normal variation in the frequency and location of human auditory cortex landmarks. Heschl's gyrus: Where is it? *Cereb. Cortex* **8:**397–406.

Loftus, W. C., Tramo, M. J., and Gazzaniga, M. S. 1995. Cortical surface modeling reveals gross morphometric correlates of individual differences. *Hum. Brain Mapp.* **3:**257–270.

Luppino, G., Matelli, M., Camarda, R. M., Gallese, V., and Rizzolatti, G. 1991. Multiple representations of body movements in mesial area 6 and the adjacent cingulate cortex: An intracortical microstimulation study in the macaque monkey. *J. Comp. Neurol.* **311:** 463–482.

Matelli, M., Luppino, G., and Rizzolatti, G. 1991. Architecture of superior and mesial area 6 and the adjacent cingulate cortex in the macaque monkey. *J. Comp. Neurol.* **311:**445–462.

Merker, B. 1983. Silver staining of cell bodies by means of physical development. *J. Neurosci. Methods* **9:**235–241.

Naito, E., Ehrsson, H. H., Geyer, S., Zilles, K., and Roland, P. E. 1999. Illusory arm movements activate cortical motor areas: A positron emission tomography study. *J. Neurosci.* **19:**6134–6144.

Ono, M., Kubik, S., and Abernathey, C. D. 1990. *Atlas of the Cerebral Sulci.* Thieme, Stuttgart.

Paus, T., Otaky, N., Caramanos, Z., MacDonald, D., Zijdenbos, A., D'Avirro, D., Gutmans, D., Holmes, C., Tomaiuolo, F., and Evans, A. C. 1996a. In vivo morphometry of the intrasulcal gray matter in the human cingulate, paracingulate, and superior-rostral sulci: Hemispheric asymmetries, gender differences and probability maps. *J. Comp. Neurol.* **376:**664–673.

Paus, T., Tomaiuolo, F., Otaky, N., MacDonald, D., Petrides, M., Atlas, J., Morris, R., and Evans, A. C. 1996b. Human cingulate and paracingulate sulci: Pattern, variability, asymmetry, and probabilistic map. *Cereb. Cortex* **6:**207–214.

Penhune, V. B., Zatorre, R. J., MacDonald, J. D., and Evans, A. C. 1996. Interhemispheric anatomical differences in human primary auditory cortex: Probabilistic mapping and volume measurement from magnetic resonance scans. *Cereb. Cortex* **6:**661–672.

Rademacher, J., Caviness, V. S., Steinmetz, H., and Galaburda, A. M. 1993. Topographical variation of the human primary cortices: Implications for neuroimaging, brain mapping, and neurobiology. *Cereb. Cortex* **3:**313–329.

Rajkowska, G., and Goldman-Rakic, P. S. 1995. Cytoarchitectonic definition of prefrontal areas in the normal human cortex: II. Variability in locations of areas 9 and 46 and relationship to the Talairach coordinate system. *Cereb. Cortex* **5:**323–337.

Roland, P. E., Fredriksson, J., Svensson, P., Amunts, K., Cavada, C., Hari, R., Cowey, A., Crivello, F., Geyer, S., Kostopoulos, G., Mazoyer, B., Popplewell, D., Schleicher, A., Schormann, T., Seppa, M., Uylings, H. B. M., de Vos, K., and Zilles, K. 1999. ECHBD, a database for functional–structural and functional–functional relations in neuroimaging. *Neuroimage* **9:**S128.

Roland, P. E., Geyer, S., Amunts, K., Schormann, T., Schleicher, A., Malikovic, A., and Zilles, K. 1997. Cytoarchitectural maps of the human brain in standard anatomical space. *Hum. Brain Mapp.* **5:**222–227.

Roland, P. E., Graufelds, C. J., Wåhlin, J., Ingelman, L., Andersson, M., Ledberg, A., Pedersen, J., Åkerman, S., Dabringhaus, A., and Zilles, K. 1994. Human brain atlas: For high-resolution functional and anatomical mapping. *Hum. Brain Mapp.* **1:**173–184.

Roland, P. E., and Zilles, K. 1994. Brain atlases—A new research tool. *Trends Neurosci.* **17:**458–467.

Roland, P. E., and Zilles, K. 1996b. Functions and structures of the motor cortices in humans. *Curr. Opin. Neurobiol.* **6:**773–781.

Roland, P. E., and Zilles, K. 1996a. The developing European computerized human brain database for all imaging modalities. *Neuroimage* **4:**S39–S47.

Roland, P. E., and Zilles, K. 1998. Structural divisions and functional fields in the human cerebral cortex. *Brain Res. Rev.* **26:**87–105.

Schleicher, A., Amunts, K., Geyer, S., Morosan, P., and Zilles, K. 1999. Observer-independent method for microstructural parcellation of cerebral cortex: A quantitative approach to cytoarchitectonics. *Neuroimage* **9:**165–177.

Schormann, T., Dabringhaus, A., and Zilles, K. 1995. Statistics of deformations in histology and application to improved alignment with MRI. *IEEE Trans. Med. Imaging* **14:**25–35.

Schormann, T., Dabringhaus, A., and Zilles, K. 1997. Extension of the principal-axes theory for the determination of affine transformations. In *Mustererkennung 1997 (19 DAGM-Symposium, Braunschweig, 15–17 September 1997)* (E. Paulus and F. M. Wahl, Eds.), pp. 384–391. Springer, Berlin.

Schormann, T., Henn, S., Bürgel, U., Engler, K., and Zilles, K. 1997. A new technique for 3-D nonlinear deformation: Application to studies of the variability of brain structures. *Neuroimage* **5:**S418.

Schormann, T., Henn, S., and Zilles, K. 1996. A new approach to fast elastic alignment with application to human brains. *Lect. Notes Comput. Sci.* **1131:**437–442.

Schormann, T., von Matthey, M., Dabringhaus, A., and Zilles, K. 1993. Alignment of 3-D brain data sets originating from MR and histology. *Bioimaging* **1:**119–128.

Schormann, T., and Zilles, K. 1997. Limitations of the principal-axes theory. *IEEE Trans. Med. Imag.* **16:**942–947.

Schormann, T., and Zilles, K. 1998. Three-dimensional linear and nonlinear transformations: An integration of light microscopical and MRI data. *Hum. Brain Mapp.* **6:**339–347.

Schormann, T., and Zilles, K. 1999. Raleyigh-Bessel distribution of nonlinear deformations in histological sections. In press.

Talairach, J., and Tournoux, P. 1988. *Co-Planar Stereotaxic Atlas of the Human Brain. 3-Dimensional Proportional System: An Approach to Cerebral Imaging.* Thieme, Stuttgart.

Thompson, P. M., Schwartz, C., Lin, R. T., Khan, A. A., and Toga, A. W. 1996. Three-dimensional statistical analysis of sulcal variability in the human brain. *J. Neurosci.* **16:**4261–4274.

Tomaiuolo, F., MacDonald, J. D., Caramanos, Z., Posner, G., Chiavaras, M., Evans, A. C., and Petrides, M. 1999. Morphology, morphometry and probability mapping of the pars opercularis of the inferior frontal gyrus: An *in vivo* MRI analysis. *Eur. J. Neurosci.* **11:**3033–3046.

Varnavas, G. G., and Grand, W. 1999. The insular cortex: Morphological and vascular anatomic characteristics. *Neurosurgery* **44:** 127–138.

Westbury, C. F., Zatorre, R. J., and Evans, A. C. 1999. Quantifying variability in the planum temporale: A probability map. *Cereb. Cortex* **9:**392–405.

White, L. E., Andrews, T. J., Hulette, C., Richards, A., Groelle, M., Paydarfar, J., and Purves, D. 1997. Structure of the human sensorimotor system. I: Morphology and cytoarchitecture of the central sulcus. *Cereb. Cortex* **7:**18–30.

Woods, R. P., Grafton, S. T., Watson, J. D., Sicotte, N. L., and Mazziotta, J. C. 1998. Automated image registration: II. Intersubject validation of linear and nonlinear models. *J. Comput. Assist. Tomogr.* **22:**153–165.

Zilles, K., Armstrong, E., Schleicher, A., and Kretschmann, H. J. 1988. The human pattern of gyrification in the cerebral cortex. *Anat. Embryol.* **179:**173–179.

Zilles, K., Schleicher, A., Langemann, C., Amunts, K., Morosan, P., Palomero-Gallagher, N., Schormann, T., Mohlberg, H., Bürgel, U., Steinmetz, H., Schlaug, G., and Roland, P. E. 1997. Quantitative analysis of sulci in the human cerebral cortex: Development, regional heterogeneity, gender difference, asymmetry, intersubject variability and cortical architecture. *Hum. Brain Mapp.* **5:**218–221.